Characterization of the main error sources of chromatic confocal probes for dimensional measurement

IOP Publishing Measurement Science and Technology
Meas. Sci. Technol. **25** (2014) 044011 (14pp) doi:10.1088/0957-0233/25/4/044011

Characterization of the main error sources of chromatic confocal probes for dimensional measurement

H Nouira[1,3], **N El-Hayek**[1], **X Yuan**[1] **and N Anwer**[2]

[1] Laboratoire Commun de Métrologie (LNE-CNAM), Laboratoire National de Métrologie et d'Essais (LNE), 1 Rue Gaston Boissier, F-75015 Paris, France
[2] Ecole Normale Supérieure de Cachan, University Research Laboratory in Automated Production (LURPA), 61 avenue du Président Wilson, F-94235 Cachan, France

E-mail: hichem.nouira@lne.fr

Received 4 November 2013, revised 29 November 2013
Accepted for publication 13 December 2013
Published 5 March 2014

Abstract

Chromatic confocal probes are increasingly used in high-precision dimensional metrology applications such as roughness, form, thickness and surface profile measurements; however, their measurement behaviour is not well understood and must be characterized at a nanometre level. This paper provides a calibration bench for the characterization of two chromatic confocal probes of 20 and 350 μm travel ranges. The metrology loop that includes the chromatic confocal probe is stable and enables measurement repeatability at the nanometer level. With the proposed system, the major error sources, such as the relative axial and radial motions of the probe with respect to the sample, the material, colour and roughness of the measured sample, the relative deviation/tilt of the probe and the scanning speed are identified. Experimental test results show that the chromatic confocal probes are sensitive to these errors and that their measurement behaviour is highly dependent on them.

Keywords: chromatic confocal probe, error sources, dimensional metrology, uncertainty budget

(Some figures may appear in colour only in the online journal)

1. Introduction

The work presented in this paper is part of the European Metrology Research Programme (EMRP) project IND10 entitled 'Optical and tactile metrology for absolute form characterization'. This project investigates measurement with a tactile micro-probe, which is still the most widely used in dimensional metrology for its simplicity, performance and universally agreed standardization. However, measurements involving contact with the sample show many limitations, including the inability to perform measurements over deformable surfaces. Non-contact optical measurement devices have therefore been developed for this matter and have shown remarkable achievements pertaining to high precision and fast rate measurement [1]. Since 2010, chromatic confocal probe instruments are included in the classification of surface texture instruments (areal-topography measurements (ISO 25178-6:2010 [2]). Along with this interesting technological advancement, the IND10 project has additionally addressed a specific issue engaging the characterization of chromatic confocal probes. Their working principle has been described by Charron [3], Leach [4], Wilson [5], Schwenke *et al* [6] and Cacace [7], and normalized in ISO 25178-602:2010 [8].

Research studies have been conducted to characterize and calibrate chromatic confocal probes, which are mostly dedicated to the measurement of form, roughness, profile and thickness. Calibration is achieved by comparing the confocal measurement with a more accurate measurement serving as a reference in order to ensure measurement traceability. In this context, Boltryk *et al* [9, 10] investigate the behaviour

[3] Author to whom any correspondence should be addressed.

of chromatic confocal probes when performing measurement on cylindrical artefacts with sinusoidal grooves. The results reveal that the confocal measurements depend on the depth of the grooves and the inclination of the flanks. However, other sources of error are disregarded and unidentified, such as the impact of the material, the reflectivity, the roughness and the shape of the sample, as well as the environmental conditions, the acquisition frequency and the scanning speed. As reported by Leach in [4], all these error sources may influence the performance of the chromatic confocal probe and particularly the maximum measurable local slope. In addition, Leach did not present any experimental test results or any evaluation of these sources.

This paper addresses the characterization of two chromatic confocal probes with measuring ranges of 20 and 350 μm with the aim of integrating them into the developed LNE's high-precision profilometer dedicated to the measurement of both roughness and surface texture of flat standards and aspherical surfaces. Measured samples can be made of steel, ceramic, aluminium or glass with different surface coating (gold, copper, aluminium, ...). To assess the measurement capability of the apparatus, the behaviour of the chromatic confocal probes and the error sources have to be identified. This identification allows for better estimation of the uncertainty budget of the high-precision profilometer. For this purpose, a new specific calibration bench has been developed. Its design has been detailed, uncertainty budget estimated and the experimental test results presented and discussed.

2. Specification of the LNE's high-precision profilometer

The high-precision profilometer used for the measurement of a variety of sample geometries and materials such as flat standards and aspherical surfaces performs three independent motions in the x-, y- and z- directions under the control of three independent laser interferometers (figure 1). Two horizontal and orthogonal high-precision guiding systems support a Zerodur table and ensure controlled dynamic operations in the XY plane. A third vertical high-precision guiding system includes an Invar metrology frame holding the measuring probe, which performs measurement and moves along the z-direction [11].

The performance of the profilometer depends on the quality of the mechanical guiding systems, the stability of the metrology frame and the behaviour of the measuring probe.

The profilometer also offers the possibility to perform *in situ* calibration; nevertheless, this calibration does not allow for as many degrees of freedom as needed to investigate the entire error sources that influence the measurement. Hence, for the calibration of the chromatic confocal probes, an independent calibration device is necessary.

3. Operating principle and need for the characterization of chromatic confocal probes

In confocal chromatic systems, an LED sends a white light beam through a lens that diffracts emerging light into spectral waves (figure 2). These spectral waves are directed towards

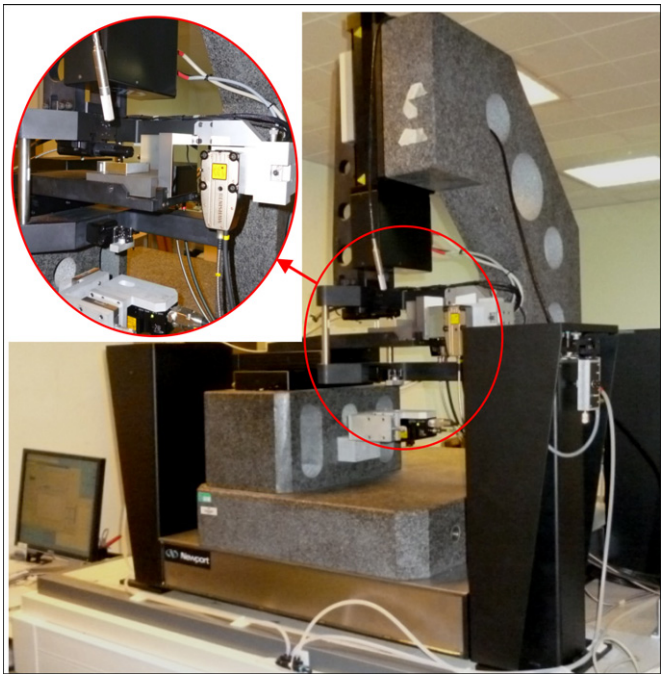

Figure 1. Photograph of the ultra-high-precision profilometer.

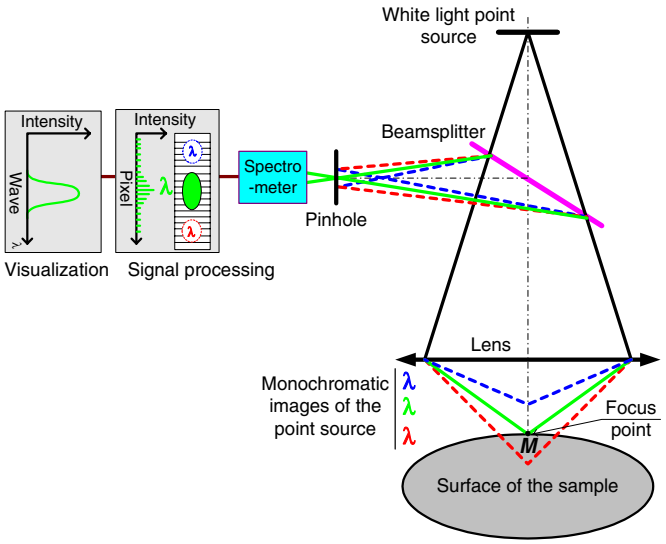

Figure 2. The working principle of the chromatic confocal probe.

the surface being measured, then reflected back and analysed in a spectrometer. Only the wavelength (λ) that is best focused on the surface of the object being measured passes through a mechanical filter called the pinhole [4–8]. This wavelength is in reality a small range of wavelengths, which will be diffracted onto a CCD camera and analysed. Hereafter, the system searches for a peak in the signal and finds the location of this peak on the CCD. Equation (1) shows how the location of the peak is related to the magnitude of the focalized point M, and therefore to the distance (d) separating the chromatic confocal probe's head from the surface being measured:

$$d = f(\lambda), \tag{1}$$

where d is the distance, λ the wavelength and f (...) the functional.

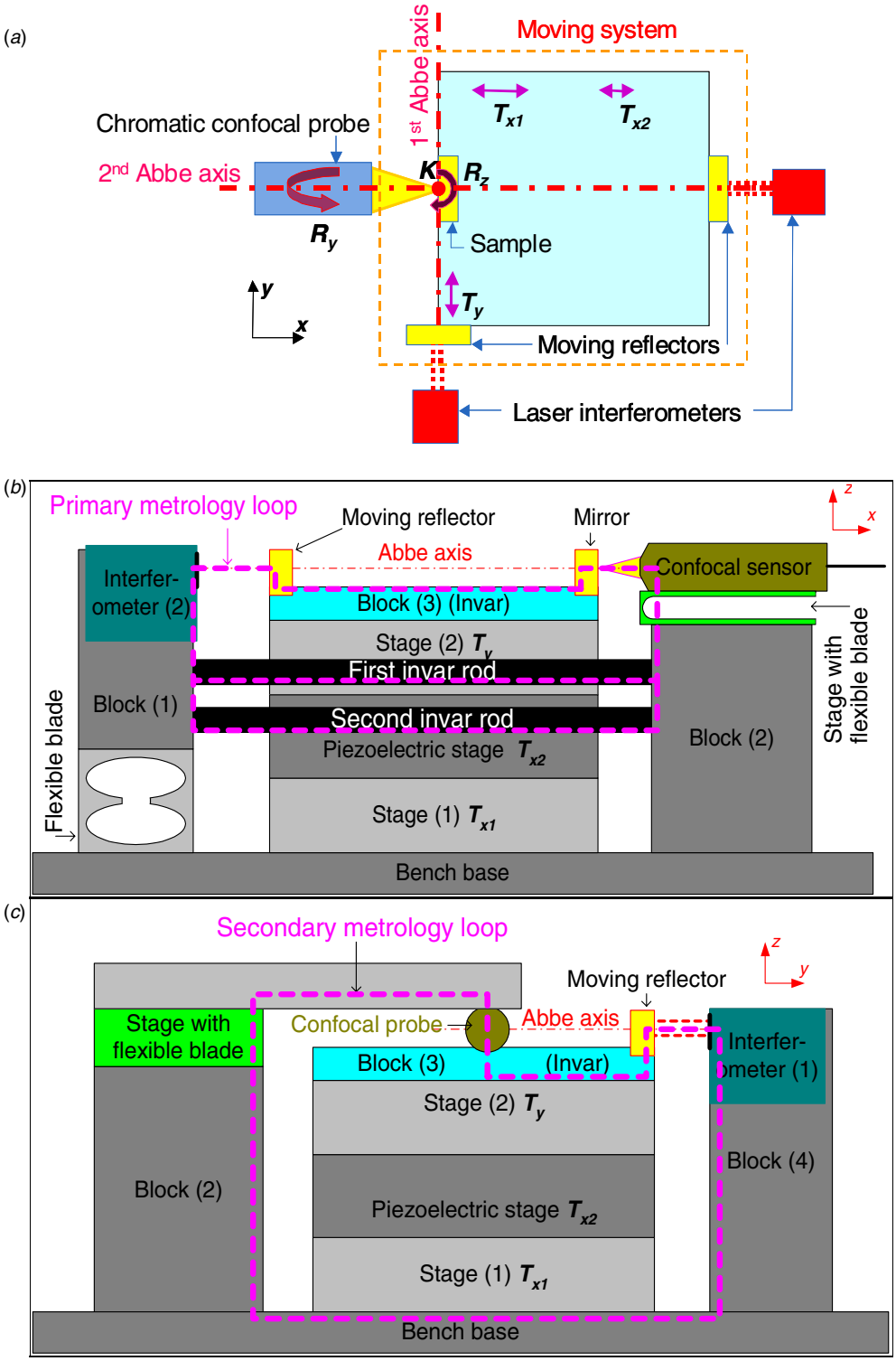

Figure 3. (*a*) Configuration of the test bench. (*b*) The primary metrology loop along the chromatic confocal probe's direction. (*c*) The secondary metrology loop in transversal direction.

The intrinsic properties of the flat standard or the aspherical surface (the material, the colour/reflectivity and the roughness), the behaviour of the optical probe, the inclination/tilt of the probe or the sample, the intensity/power of the light source, the acquisition frequency and the scanning speed may influence the maximum measurable local slope ([4] and ISO 25178-602:2010 [8]). The surface roughness creates a diffuse reflection of light. The small part that is reflected should be enough to detect the peak position in the intensity curve recorded in the spectrometer. The variation of the percentage of reflected light may affect the quality of the spectrum (intensity curve) [4].

Consequently, a new calibration bench, independent of the profilometer, is developed to evaluate all these error sources. According to the behaviour of the chromatic confocal probes on this bench, corrections have to be taken into account in the software of the high-precision profilometer, in order to improve its measurement capability.

4. Experimental set-up

To characterize the chromatic confocal probes, a new calibration bench is designed that ensures two independent motions (T_x and T_y) along the x- and y-axes (figure 3(a)). Along the x-axis, nanometric or/and micrometric motions (T_{x1} and T_{x2}, where $T_x = T_{x1} + T_{x2}$) can be generated using two independent high-precision mechanical stages. The first one produces a micrometric motion step using a manual guiding system stage with a travel range of 63 mm. The second mechanical stage incorporates a piezoelectric actuator, which is used with electronic feedback, and a mechanical structure based on four flexible blades so that it limits any hysteresis phenomenon. This stage automatically and quasi-perfectly generates nanometric motion steps of 5 nm over the entire travel range of 90 μm. An automatic mechanical stage with the entire travel range of 50 mm and a minimal sub-micrometric motion step of 0.7 μm ensures the translation T_y (figure 3(a)).

A manual tangent stage based on flexible blades guarantees the rotation R_y around the y-axis and a manual rotary stage ensures the rotation R_z of the part around the z-axis, in particular around point K. The rotation R_y of the probe is performed around a horizontal axis parallel to the y-axis and crossing the indicated point K. Point K corresponds to the intersection of the first and second Abbe axes. Therefore, the first Abbe axis is mingled with the laser interferometer beam and the chromatic confocal probe's axis. The second Abbe axis corresponds to the intersection of the horizontal plane OXY crossing the first Abbe axis and the vertical plane that is intermingled with the scanning point.

Two independent Renishaw laser interferometers with sub-nanometric resolution are used as references to measure the displacements T_x and T_y separately. Each laser interferometer is focused on a moving plane reflector (mirror) made of Zerodur, which has high surface quality and a flatness of $\lambda/20$. The alignment between the laser interferometer and the mirror is ensured by a specific procedure based on an external sensitive contact measurement.

The experimental tests are performed inside the LNE cleanroom where temperature and humidity are controlled respectively to 20 ± 0.3 °C and $50 \pm 5\%$ RH. To ensure better homogeneous temperature during the test, the instrument is also enclosed in an aluminium shell and installed on an optical table with advanced vibration isolation features to avoid low-frequency vibrations.

All the motions are controlled and driven using the developed LabView interface. A systematic and synchronous recording of the laser interferometers, chromatic confocal probe, temperature, hygrometry and pressure data is carried out during the test.

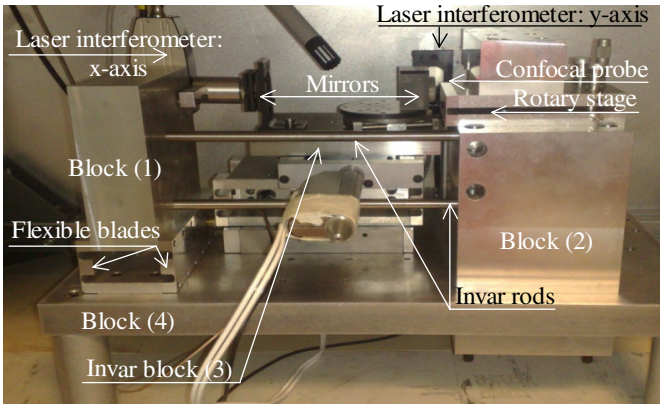

Figure 4. Photograph of the test bench.

4.1. Metrology analysis of the developed set-up

Figure 3(b) shows a schematic front-view sketch of the test bench. It is constituted of a block that holds the x-laser interferometer on one side (2), a block that holds the chromatic confocal probe on the other side and the Zerodur table (block (3)) performing 2D translations. In order to apply the dissociated metrological structure principle [12, 13], the block (1) containing the laser interferometer (2) is decoupled from the bench base, made of aluminium, using two flexible blades. Moreover, two Invar rods have been installed to rigidly link both measuring entities (block (1) and block (2)) and shorten the primary metrology loop shown in figures 3(b) and 4. Invar is known to have a coefficient of thermal expansion around 0.7 μm (m °C)$^{-1}$, which is remarkably smaller than the coefficient of thermal expansion of aluminium (22 μm (m °C)$^{-1}$). The block (3) supporting the sample is also made of Invar material, which increases the rigidity of the metrology frame. Therefore, any thermal expansion of the bench base slightly influences the primary metrology loop.

The secondary metrology loop passes through the bench base, blocks (2) and (4), the chromatic confocal probe and the laser interferometer (1) along the y-direction. Since this loop is shorter than the primary one and is not as influential, it could be kept as in figure 3(c). This last loop is considered only for checking the transverse motion error of the test bench during the experiment.

4.2. Performance of the test bench

The uncertainty and measurement traceability present a pyramidal structure as in figure 5(a). Then, two kinds of errors that influence the measurement can be distinguished: the systematic errors that can be characterized and compensated for and the random errors that represent uncorrectable errors, which can only be diminished by increasing sampling density. For the experimental set-up, the identification of the sources of errors (figure 5(b)) affecting the results should be done to reduce the effect of some of them.

For the general case described by the measurement model in equation (2), considering the coefficient of uncertainty of each parameter $u(x_1), \ldots, u(x_N)$ and based on the GUM

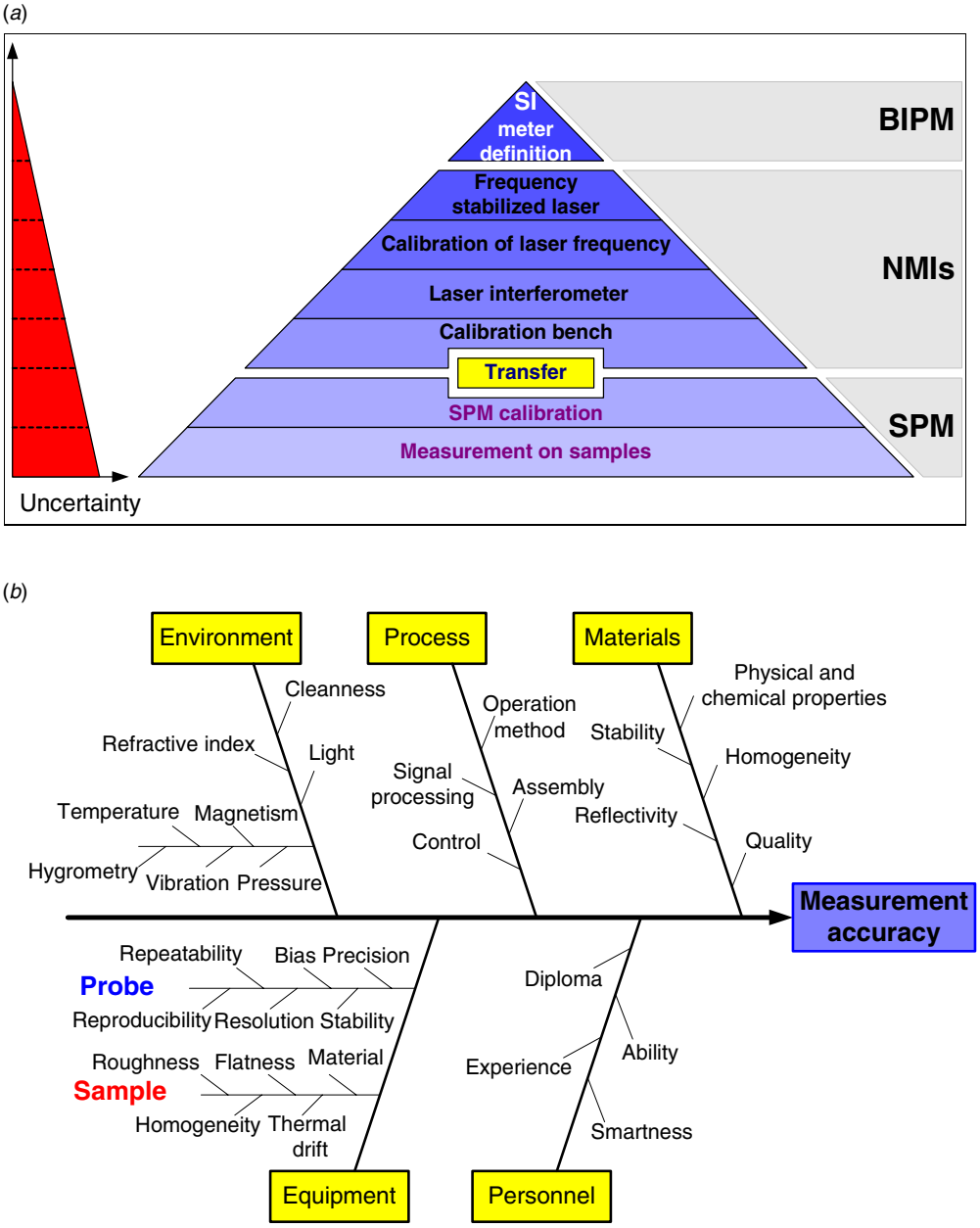

Figure 5. (*a*) Measurement traceability pyramid relative to dimensional measurements. (*b*) The error sources of the measurement uncertainty (SPM: scanning probe measurement).

approach [14], the uncertainty propagation can be given by equation (3):

$$y = f(x_1, x_2, \ldots, x_N) \tag{2}$$

$$u_c^2(y) = \sum_{i=1}^{N} \left(\frac{\partial f}{\partial x_i}\right)^2 u^2(x_i) + 2\sum_{i=1}^{N-1}\sum_{j=i+1}^{N} \frac{\partial f}{\partial x_i}\frac{\partial f}{\partial x_j} u(x_i, x_j). \tag{3}$$

4.2.1. Thermal expansion of the test bench. Referring to the Vaisala instrument, the recorded variation of temperature ΔT in air is less than 0.3 °C inside the LNE cleanroom and the corresponding variation in the material's temperature is estimated to be not more than 0.01 °C. Such variation of the temperature influences the mechanical behaviour of the bench structure, which can be estimated by the following formula (equation (4)):

$$\Delta W = \alpha W \Delta T, \tag{4}$$

where α is the thermal expansion coefficient and W the length.

4.2.2. Thermal variation of the wavelength. The wavelength of the laser interferometer λ_v depends on temperature (T), humidity (RH), pressure (p), the dead path (ΔP) and the refractive index (n_{air}) [15]. These parameters have associated uncertainties, which are propagated using the GUM approach. The propagated uncertainty over the displacement measured (ΔL) by the laser interferometer can be approximated as in equation (5):

Table 1. The uncertainty budget of the test bench when performing measurement.

Error sources	Estimation	Individual uncertainty	Sensibility	Global uncertainty (nm)
Instability of the set-up				
Thermal expansion	$\Delta T = 0.01\ ^\circ$C			2.17 (nm)
Uncertainty of the interferometric measurement				
Refractive index	$n_{air} = 1.00025137$	1.6×10^{-7}	ΔL	$1.6 \times 10^{-7}\ \Delta L$
Temperature	$T = 20\ ^\circ$C	0.15 °C	$9.6 \times 10^{-7}\ \Delta L/^\circ$C	$1.5 \times 10^{-7}\ \Delta L$
Pressure	1013.25 hPa	25 Pa	$2.7 \times 10^{-9}\ \Delta L$/Pa	$67.5 \times 10^{-9}\ \Delta L$
Relative humidity	50%	0.8%	$8.5 \times 10^{-9}\ \Delta L/\%RH$	$7 \times 10^{-9}\ \Delta L/\%RH$
Cosine error	2 μm for 8 mm		1	$3.51 \times 10^{-6}\ \Delta L$
Abbe error	200 μrad for 63 mm		1	$1.59 \times 10^{-6}\ \Delta L$
Dead path axis 1	45 mm	0.003 m	$\Delta n_{air}/n_{air}$	0.05
Dead path axis 2	15 mm	0.003 m	$\Delta n_{air}/n_{air}$	0.05
Resolution	0.04 nm/bit	0.04	1	0.04
Nonlinearity	2 nm	2	1	2.0
Set-up derivation	0.6 nm	0.6	1	0.6
Interferometric uncertainty	For a distance ΔL of 90 μm			$\sim$ 2.1 (nm)
Uncertainty of the confocal chromatic measurement				
Cosine error	2 μm for 8 mm		1	$1.18 \times 10^{-5}\ \Delta L$
Abbe error	200 μrad for 63 mm		1	$1.59 \times 10^{-6}\ \Delta L$
Resolution	12 nm	12	1	12
Uncertainty of the chromatic confocal probe	For a distance ΔL of 90 μm			$\sim$ 12 (nm)

$$u(\Delta L) \approx \sqrt{\left(\frac{\Delta n_{air}}{n_{air}}\right)^2 u^2(\Delta P)} \approx 1.6 \times 10^{-7} \times \Delta L. \quad (5)$$

According to this equation, the air parameters in the dead path, especially the temperature, are responsible for the accuracy of the measured displacement (ΔL).

4.2.3. Cosine error. The cosine error of the measuring entities is described by an angle θ between the motion direction and the laser interferometer's axis of measurement. Such an error can be evaluated by quantifying the straightness of the motion and the acceptance angle of the laser interferometer (equation (6)). For the chromatic confocal probe, the cosine error can reach much higher values (equation (7)):

$$u(\cos_{laser}) = \Delta L \cdot \frac{\theta^2}{2} = 3.51 \times 10^{-6} \Delta L \quad (6)$$

$$u(\cos_{confocal}) = \Delta L \cdot \frac{\varphi^2}{2} = 1.18 \times 10^{-5} \Delta L, \quad (7)$$

where φ represents the angle between the probe axis and the motion direction.

4.2.4. Abbe error. The Abbe error is related to the offset and the small angle deviation β between the measurand and the axis of measurement, and given by equation (8). For both the laser interferometer and the chromatic confocal probe, the Abbe errors are usually similar and depend on the tolerance of the mechanical manufacturing samples and the assembly precision:

$$u_{Abbe} = \Delta L \times \tan(\beta) \approx \Delta L \times \beta. \quad (8)$$

4.2.5. Resolution of the laser interferometers and the chromatic confocal probe. The resolution of the laser interferometer is limited by the performance of the Heidenhain counting card IK220. This electronic card accepts a 12-bit interpolation. Considering the four-way laser instrument, this resolution becomes equal to 0.04 nm. For the chromatic confocal probe, the resolution is reported to be around 12 nm.

4.2.6. Uncertainty budget. The budget of uncertainty is detailed in table 1 and reveals that the main error sources are caused by the thermal expansion and the resolutions of the measuring elements. Thus, the resolution of the chromatic confocal probe represents the major error source; however, the bench presents a nanometric level of accuracy.

Three main rules have to be considered while mounting the apparatus: respecting the orthogonality between the x and y motions, the rectilinear motion of the linear stages and the alignment of the laser interferometers with their respective reflectors.

5. Error sources impacting the behaviour of the two chromatic confocal probes

The impact of the previously described error sources is evaluated through the following pre-defined tests.

- Test of motion along the x-axis (T_x): this degree of freedom corresponds to the axial motion of the confocal probe with respect to the flat sample. The evaluation of T_x gives an idea about the residual errors and the sensitivity of the probe.
- Test of motion along the y-axis (T_y): this degree of freedom corresponds to the transverse motion of the chromatic confocal probe axis from the generatrix of the cylindrical artefact. The evaluation of T_y gives an idea about the influence of the transverse motion error on the measurement.

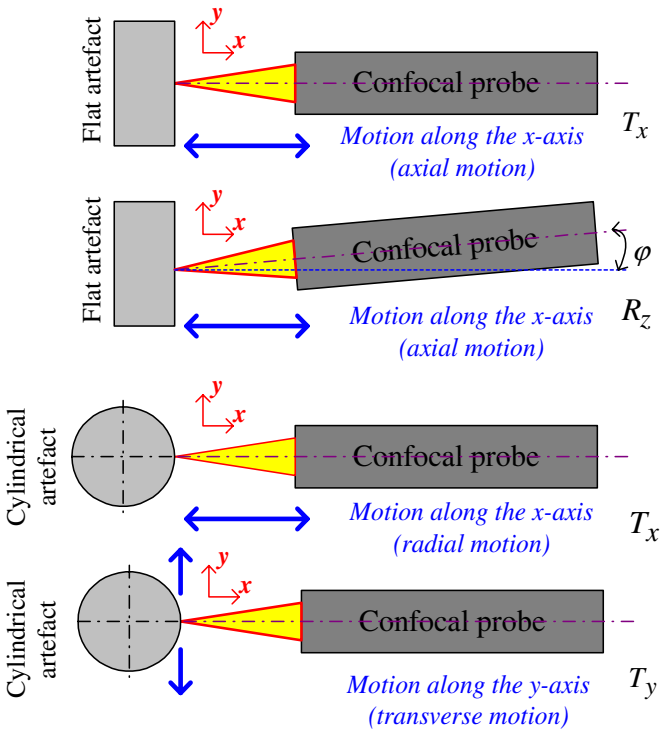

Figure 6. Description of the different tests.

- Test of rotation about the z-axis (R_z): this degree of freedom corresponds to the tilt of the confocal probe axis about the vertical axis.

Rotation R_x about the x-axis is redundant due to the axial symmetry of the probe. Rotation R_y about the y-axis presents an impact on the measurement but it is not investigated since it is similar to rotation R_z. The motion T_z along the z-axis does not change the relative distance between the probe and the sample and is therefore disregarded.

Since the chromatic confocal probes are going to be used for the measurement of flat standards (with or without harmonic undulation) and optical curved surfaces in dynamic operation mode, four experimental configurations are proposed (figures 6(*a*)–(*d*)). When using a flat sample (Zerodur mirror with different surface coatings and gauge blocks), the motions along the x- and y-axes are named axial and transverse motions respectively. For a cylindrical artefact (plug gauge), the motions along the x-, y- and z-axes are named radial, transverse and axial motions, respectively.

6. Approximation method

The methods that map corresponding control points as closely as possible to one another are called the approximation methods [16]. The information available includes the position of N corresponding control points in two images of the same sense (x_i, y_i), (X_i, Y_i), $i = 1, \ldots, N$.

Given N measurements of the form (x_i, y_i), determine a transformation function f such that when the coordinates of a control point in the reference image are applied, this function estimates the Y-component of the corresponding control point in the sensed image. Traditionally in image registration, f is taken to be a polynomial, and the parameters of the polynomial are determined by the least-squares method. However, in this paper, the Forsythe orthogonal polynomial method is applied as an alternative to the least-squares method in order to provide a more stable and accurate solution [17].

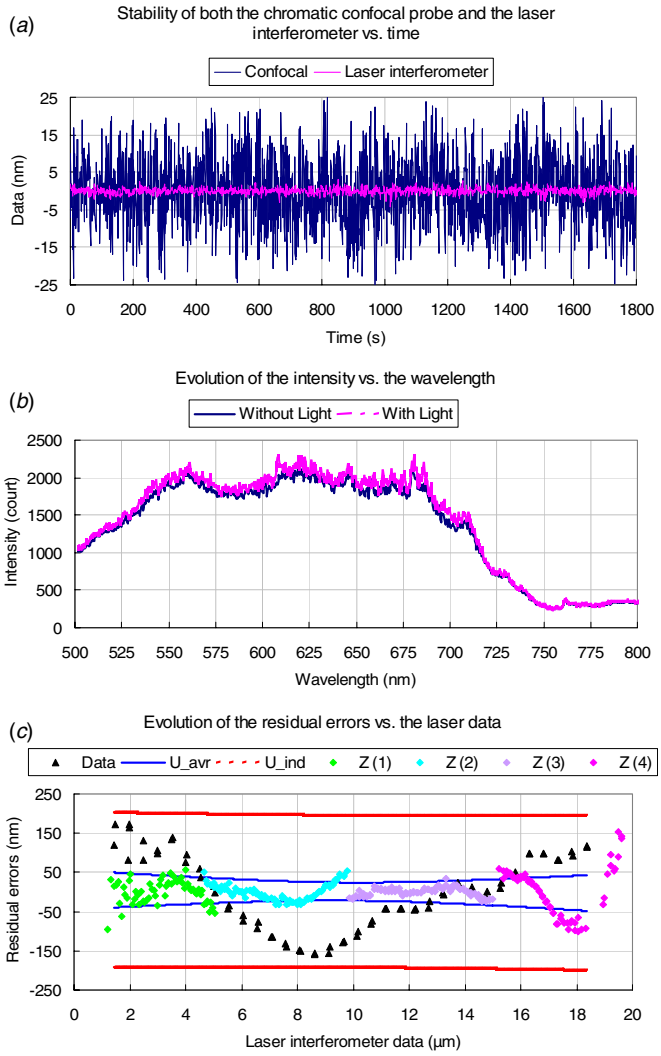

Figure 7. (*a*) The stability of the interferometer. (*b*) Spectrum power density from 500 to 800 nm. (*c*) The residual errors of the partial and entire ranges.

7. Experimental test results

7.1. Chromatic confocal probe of 20 µm working range

To accurately characterize the chromatic confocal probe, firstly, the laser interferometers stability tests are performed over half an hour. These tests are also helpful in detecting the fluctuations in the cleanroom's environmental conditions. The laser interferometer residuals present a Gaussian distribution and their stability is observed to be within 2 nm (figure 7(*a*)).

Secondly, the effect of ambient light on the chromatic confocal probe's measurement is also investigated. The power intensity is measured by a power spectral meter within the range of 500–800 nm. The intensity evolution of the chromatic

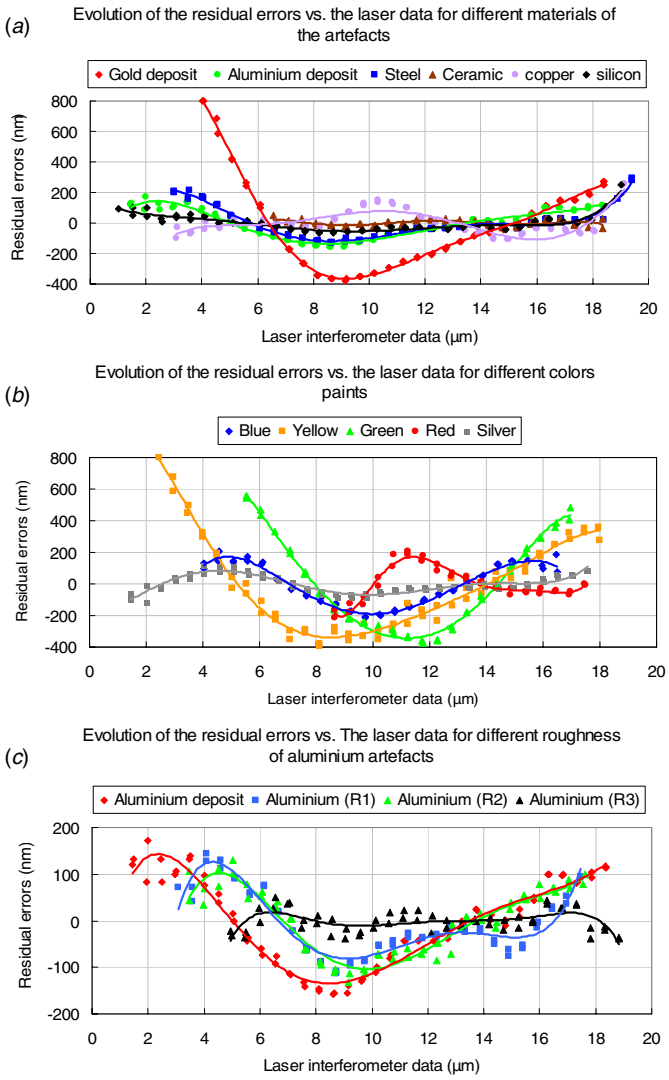

Figure 8. (*a*) Impact of the materials on the behaviour of the 20 μm confocal probe versus the interferometer data. (*b*) Impact of the colours on the behaviour of the 20 μm confocal probe versus the interferometer data. (*c*) Impact of the roughness on the behaviour of the probe versus the interferometer data.

confocal probe's light is measured with and without light inside the cleanroom. The recorded results are similar and are not influenced by ambient light as shown in figure 7(*b*).

Thirdly, the linearity of the chromatic confocal probe is evaluated using the developed calibration bench in a step-by-step procedure. The recorded data along the entire working range are approximated by a piecewise linear model. The linearity test is achieved again at different partial ranges to identify the best working range. Four partial ranges are selected as follows: 0–5, 5–10, 10–15 and 15–20 μm. Each test is performed over four 80-step cycles when the chromatic confocal probe is focused on an aluminium-deposited mirror. If the chromatic confocal probe is calibrated along the entire travel range, the residual errors (difference between the experimental and linear model data) vary between ± 150 nm (figure 7(*c*)). However, by calibrating the chromatic confocal probe over the partial ranges, the residual errors decrease and vary around ± 50 nm, except when the travel range exceeds

Table 2. Roughness of the tested aluminium materials.

	Roughness parameter R_z (μm)	Standard deviation σ (μm)
Aluminium deposit	0.020	0.0004
Aluminium *R*1	2.50	0.15
Aluminium *R*2	4.40	0.70
Aluminium *R*3	6.50	0.50

18 μm. The evolution of the individual uncertainty presents hyperbolic behaviour and reveals that it is more interesting to use the probe over a smaller travel range near the middle, i.e., from 5 to 15 μm.

The linearity test is also performed with different kinds of materials (aluminium, steel, gold, copper, silicon and ceramic), which have different absorption and reflection values with respect to the wavelengths in the white light source. The average reflectance values of the selected materials are respectively equal to 93%, 53%, 92%, 60%, 30% and 95%. In figure 8(*a*), the residual errors corresponding to the gold-deposited mirror are too high and values near the start seem to be 'compressed', and the useful range for the gold-deposited mirror is not as large compared to other materials. The ceramic material shows remarkable performance due to the small associated residuals but is limited to a smaller travel range compared to all the other tested materials. The remaining four materials, silicon, copper, steel and aluminium, behave approximately the same with a maximum working range and medium associated residuals.

Since the observed behaviour is different, the impact of colour is investigated. Five colours are chosen for the colour test: yellow, silver, red, blue and green. Results are presented in figure 8(*b*). The test reveals that colour paints do not exhibit similar behaviour. For instance, if we consider the red colour, all wavelengths are absorbed except for the wavelength corresponding to the red colour. That is why, from 0 to nearly 10 μm, there is no signal for the red colour sample. The range of 400–500 nm wavelengths, which correspond to the partial range from 0 to 8 μm, matches with blue and violet colours. Both yellow and silver behave the same as the gold-deposited mirror and the aluminium-deposited mirror, which proves that a certain amount of the wavelengths is absorbed by the test sample. For the same measuring range, it seems that the chromatic confocal probe's behaviour highly depends on the colour rather than on the material.

The linearity of the probe is further investigated with various selected roughness aluminium surfaces measured by the high-precision profilometer using a sensitive tactile probe. Both values of roughness R_z and standard deviation (σ) are the results of the average of 16 measurements over a distance of 0.8 mm (table 2). Based on figure 8(*c*), it is obvious that the effective working range depends on the roughness of the sample. Adding roughness induces a less effective working range. This is related to the power density spectrum for which the power density could not reach the minimum detectable value in the power spectrometer.

The influence of the angle between the probe and the flat samples is investigated within the range of $\pm 16°$.

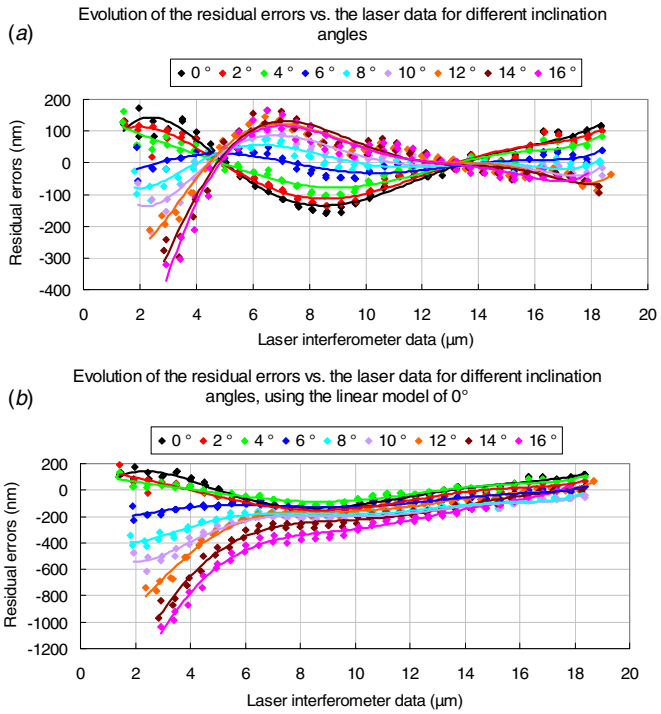

Figure 9. (*a*) Impact of the inclination angles on the residual errors versus the interferometer data. (*b*) Impact of the angles on the residual errors obtained using the linear model of 0° versus the interferometer data.

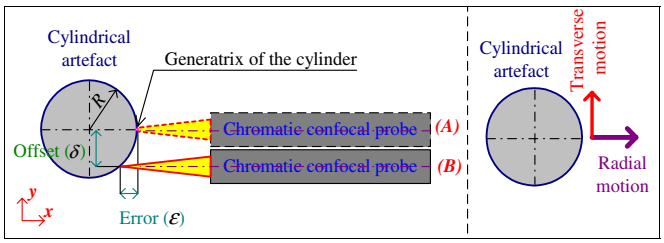

Figure 10. Description of the transverse offset test.

Eighteen measurements are performed as in figure 6(*b*) and the linearization parameters are calculated for each of them. The residual errors are deduced and the results are presented in figure 9(*a*). Since the results from 0° to −16° are symmetric to the ones between 0° and 16°, only results from 0° to 16° are presented here. When increasing the angle values, the residual errors decrease to less than ±50 nm at 6°, then increase again. Up until 16°, the residual errors vary between −400 and 130 nm. With the increase in the angle, the power density of each wave that is reflected back to the chromatic confocal probe decreases since the reflected beam approaches the edge of the chromatic confocal probe's detector. That is the reason why at 16° the starting value has large residuals compared to the residuals at 0°.

Since the error motion of the mechanical guiding systems of the apparatus varies during operation [13], it induces an unknown variation in the inclination, usually much less than 1°, of both the sample and supporting table. In other applications where a part with v-grooves is measured, the problem of relative inclination between the probe and the surface is also there. This relative inclination is not normally considered in

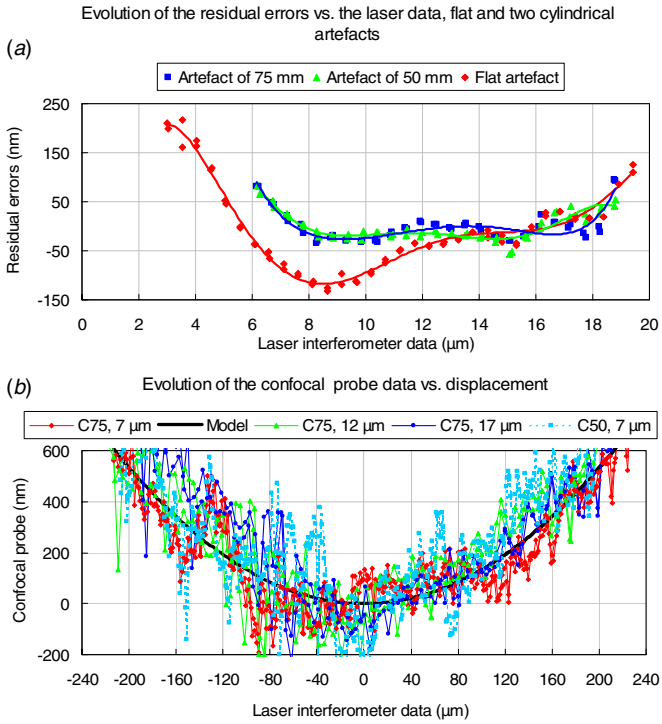

Figure 11. (*a*) The residual errors of 50 mm cylinder, 75 mm cylinder and flat sample versus the *x*-axis laser interferometer data. (*b*) Influence of the geometry/shape of the sample on the chromatic confocal probe measurement. The results are presented according to *y*-displacement measured by the *y*-axis laser interferometer, perpendicular to the chromatic confocal probe's axis.

the software and it is for this reason that calibration is a pre-requisite. To identify the impact of unconsidered inclination of the sample on the behaviour of the chromatic confocal probe, only one identified set of linearization parameters will be used to handle all the performed tests. All the measurements are re-analysed using only the linearization parameters identified with the test achieved at 0°, and the results are presented in figure 9(*b*). These results reveal that the unconsidered inclination correction dramatically affects the behaviour of the chromatic confocal probe of 20 μm, especially at the beginning of the working range zone (1–10 μm range). Henceforth, such error should be taken into account if we reach measurements of nanometric level of accuracy.

Since the measurement of optical aspherical lenses of small dimensions is to be performed on the high-precision profilometer, the impact of the shape of the sample on the behaviour of the chromatic confocal probe should be investigated. The probe is focused on two cylindrical artefacts with diameters of 50 and 75 mm, respectively. The linearity tests are completed when the probe is focused on the generatrix of the cylinder as in figure 6(*c*). The results reveal that the travel range of the probe is higher when it is focused on the steel flat sample (figure 11(*a*)). However, if we consider the same working range for the three tests, the residual errors perform perfectly the same.

The evaluation of the impact of the shape of the artefact on the behaviour of the confocal probe is completed by moving the chromatic confocal probe, while it is focused on cylindrical

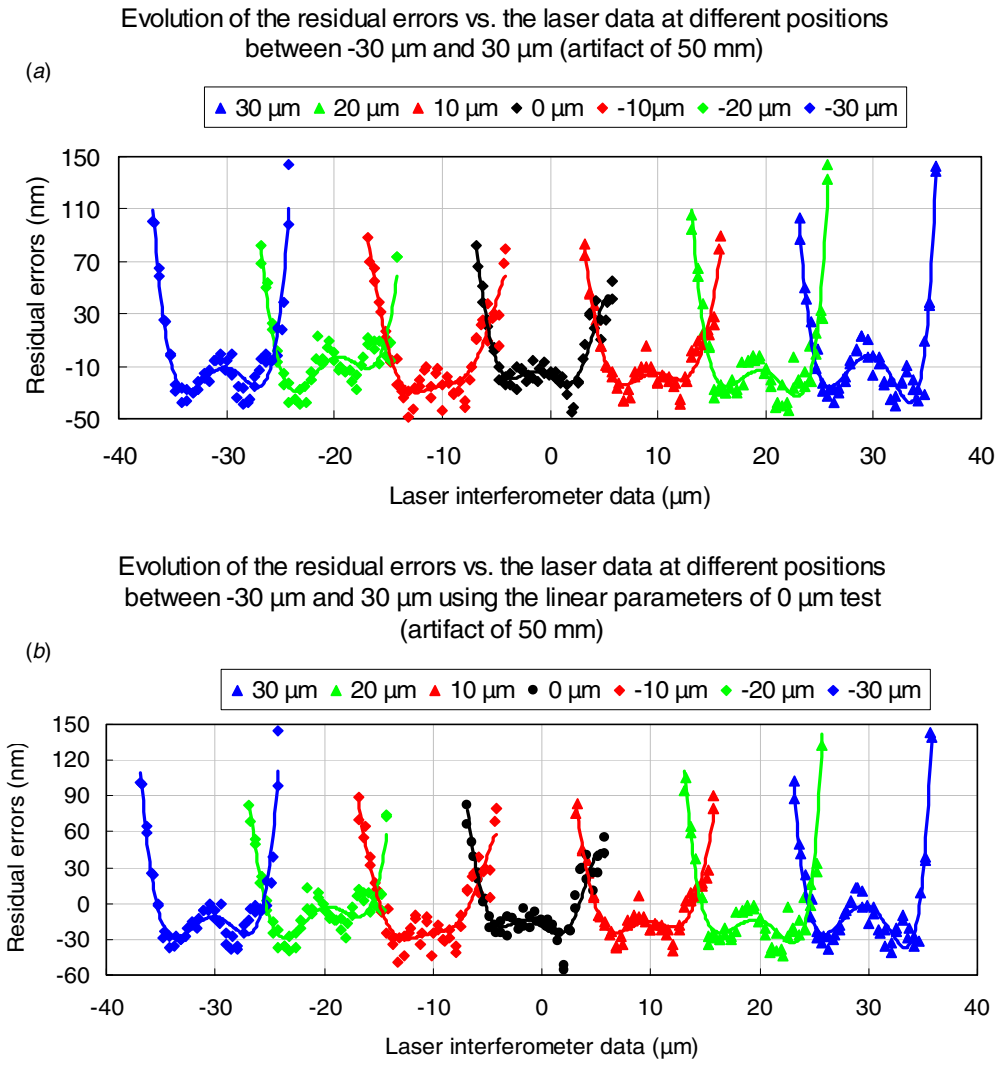

Figure 12. (*a*) Evolution of the residual errors when the probe is focused on the 50 mm cylinder at different transverse positions versus the interferometer data. (*b*) Evolution of the residual errors when using the 0 μm model versus the interferometer data from -30 to 30 μm.

artefacts, along the *y*-axis and over a range of ± 200 μm. The cylindrical artefact is selected here since it is easier to know its theoretical model. Then, the position corresponding to $y = 0$ μm represents the probe when it is focused on the generatrix of the cylindrical artefact. The experimental results are compared to the theoretical model (equation (9)) detailed in [18], obtained when the probe undergoes a transverse motion and is located at position (B) instead of position (A) (figures 10 and 6(*d*)):

$$\varepsilon = \delta^2/2R, \tag{9}$$

where R is the radius of the cylinder and δ is the offset (figure 10).

In order to perform the transverse tests as presented in figure 6(*d*), only the motion along the *y*-axis is generated. The tests are achieved with three values of the gap: 7, 12 and 17 μm and two cylinder diameters: 50 and 75 mm. To obtain more accurate results, the error motions of the mechanical stage are compensated using the indications given by the *x*-axis laser interferometer.

The comparison of both experimental and theoretical results for the 50 mm diameter cylinder is illustrated in figure 11(*b*). Agreement between the model and the experiment is observed despite the noise, which is slightly high (a range of 300 nm peak-to-valley).

Different linearity tests are also carried out over the entire travel range of the chromatic confocal probe for many transverse offset values between the probe axis and the generatrix of the cylindrical artefact with a step of 10 μm. The black curve corresponds to the case where the probe is focused on the generatrix of the cylinder (figure 12(*a*)). The two red curves correspond to the cases where transverse offsets of 10 and -10 μm between the probe axis and the generatrix of the cylinder are fixed. For this new configuration, the residual errors and uncertainties have slightly increased. Like the red curve, the green and blue curves show similar behaviour. The residual errors produced by the transverse offset of 30 μm are less than 150 nm.

When using the high-precision profilometer for measuring an aspherical lens, it is too complicated to locate the transverse position of the probe within a range of 10 μm. For this

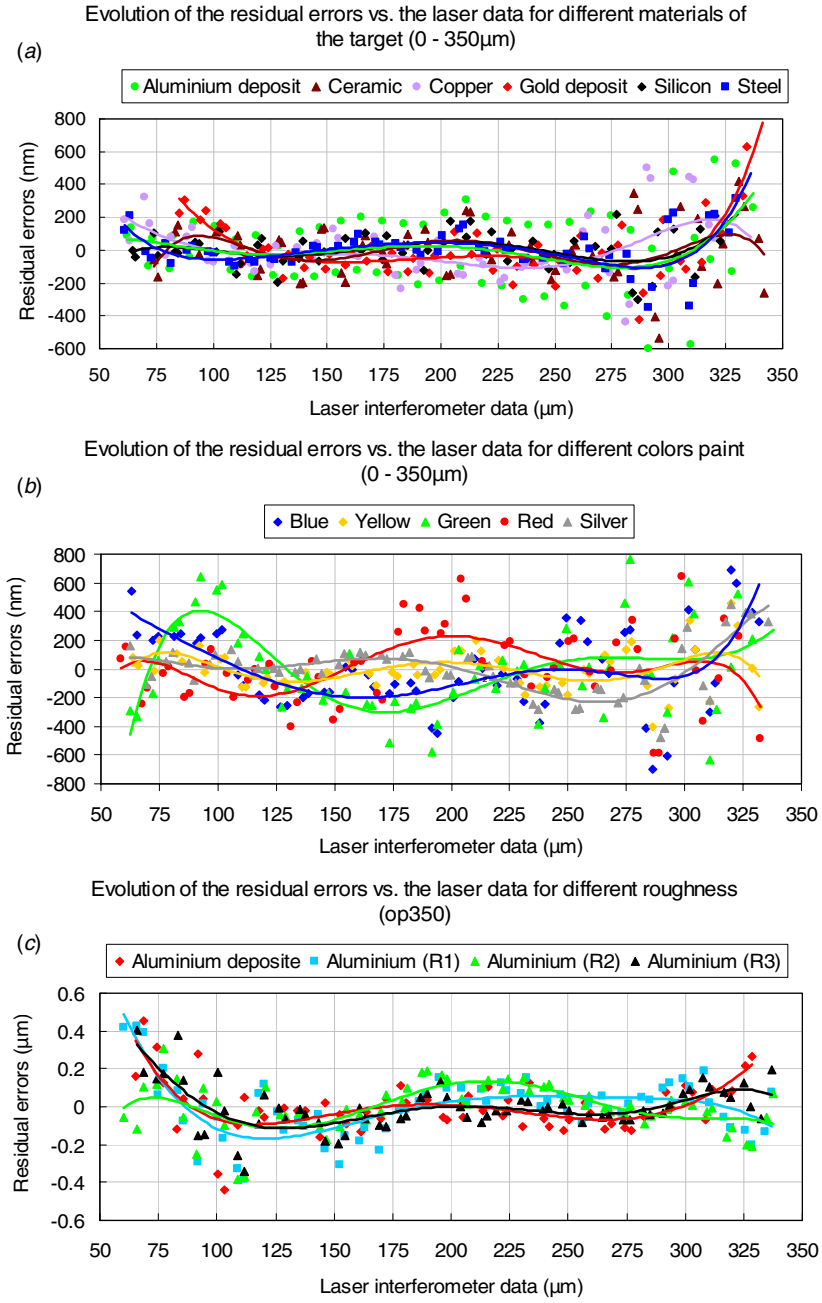

Figure 13. (*a*) Impact of the materials on the behaviour of the 350 μm chromatic confocal probe versus the interferometer data. (*b*) Impact of the colours on the behaviour of the confocal 350 μm confocal probe versus the interferometer data. (*c*) Impact of the roughness on the behaviour of the probe versus the interferometer data.

reason, all the data are processed again using the linearization parameters of 0 μm to identify the impact of this lack of knowledge on the results. From figure 12(*b*), the obtained results present similar behaviour to those obtained using their own model.

7.2. Chromatic confocal probe of 350 μm working range

The experiment is repeated for the chromatic confocal probe of 350 μm travel range. The material, colour and roughness of the flat sample slightly impact the residual errors (figures 13(*a*)–(*c*)), which vary in a bandwidth of $\pm$ 600 nm.

The influence of the angle between the probe and the flat sample is investigated within the range of $\pm 24^\circ$, but only the results from 0° to 24° are presented here. From figure 14(*a*), it can be seen that the residual errors are always within $\pm$ 600 nm, but the working range becomes smaller when the angle exceeds 22°. The test is repeated again for a partial travel range between 170 and 230 μm. The results presented in figure 14(*b*) reveal that the acceptance angle of the probe becomes much higher, reaching 28°, and that the residual errors decrease to $\pm$ 200 nm, except when the angle exceeds 24°.

The impact of the sample's shape (cylindrical artefact) on the behaviour of the probe is investigated and both

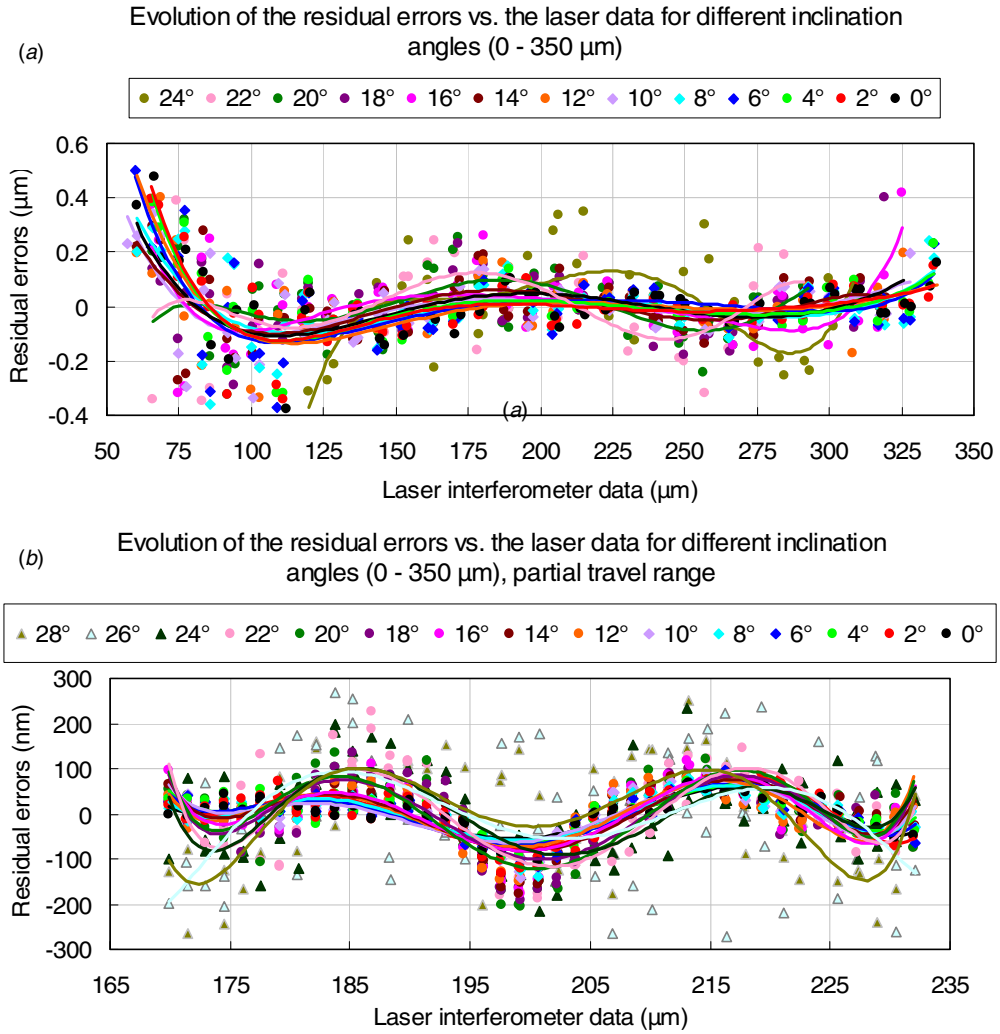

Figure 14. (*a*) Impact of the inclination angles on the residual errors versus the interferometer data. (*b*) Impact of the inclination angles on the residual errors obtained using the linear model of 0° versus the interferometer data.

experimental and theoretical results are compared. They are in good agreement (figure 15(*a*)). However, when the diameter of the cylindrical artefact decreases from 75 mm to 50 mm, the amplitude of the noise increases from 500 nm to 1200 nm (figure 15(*b*)).

For a working range of 60 μm, the effect of the transverse offset of the probe's axis of ± 30 μm with respect to the generatrix of the cylindrical artefact is investigated. The obtained results reveal that the residual errors range between ± 150 nm (figure 16(*a*)). If we use the linearization parameters at 0 μm for all, the residual errors are always similar to those obtained when using their own linearization parameters (figure 16(*b*)).

7.3. Impact of the scanning speed

The impact of the scanning speed on the behaviour of both chromatic confocal probes is explored. For the smaller range chromatic confocal probe, the scanning speed varies between 0.1 and 0.3 μm s^{-1} and the linearity tests are performed as in figure 6(*a*). The results illustrated in figure 17(*a*) reveal that the residual errors are similar (± 200 nm), but slightly higher than the previous residual errors obtained when the probe is employed following the step-by-step mode (figure 7(*c*)). The travel range is reduced and is equal to 14 μm (figure 17(*b*)) instead 17 μm as in figure 7(*c*). For the chromatic confocal probe of 350 μm, the scanning speed varies between 0.1 and 1 μm s^{-1}. The results disclose that the residual errors are similar and are in accordance with the previous residual errors obtained when the probe is employed following the step-by-step mode (figure 13(*a*)). However, when the scanning speed is equal to 1 μm s^{-1}, the travel range is reduced.

7.4. In situ calibration of the chromatic confocal probe of 350 μm on the high-precision profilometer

The probes can also be calibrated *in situ*, however, with limited degrees of freedom and a limited extent of calibration parameters. The chromatic confocal probe of 350 μm is *in situ* calibrated, and only the test of linearity versus scanning speed was performed. It seems very difficult to perform and compensate a part of the errors that influence the behaviour of the chromatic confocal probe. The obtained new data are linearized by 2048 linear models, without any averaging. Then, the linearization parameters are calculated separately over 2048 partial ranges to cover the whole travel range of 350 μm.

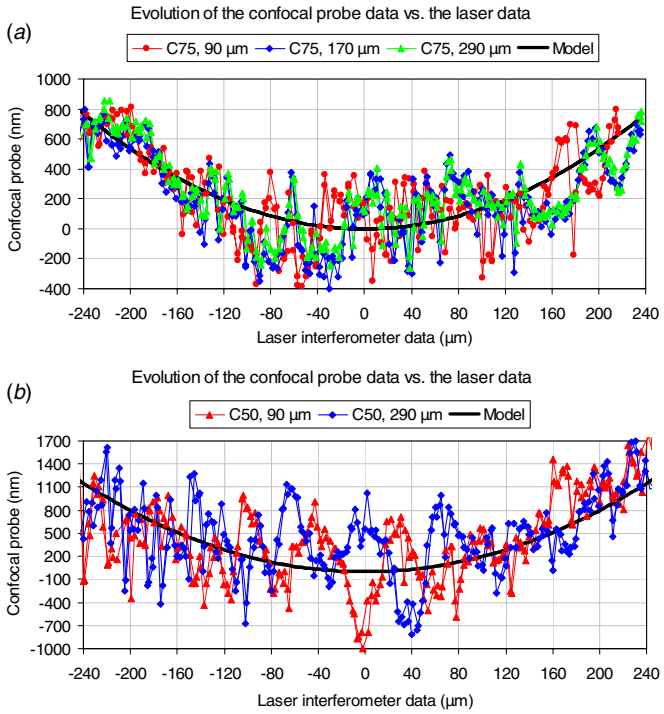

Figure 15. (*a*) Influence of the sample geometry on the chromatic confocal probe measurement when using the 75 mm cylinder made of steel. (*b*) Influence of the sample geometry on the chromatic confocal probe measurement when using the 50 mm cylinder made of steel.

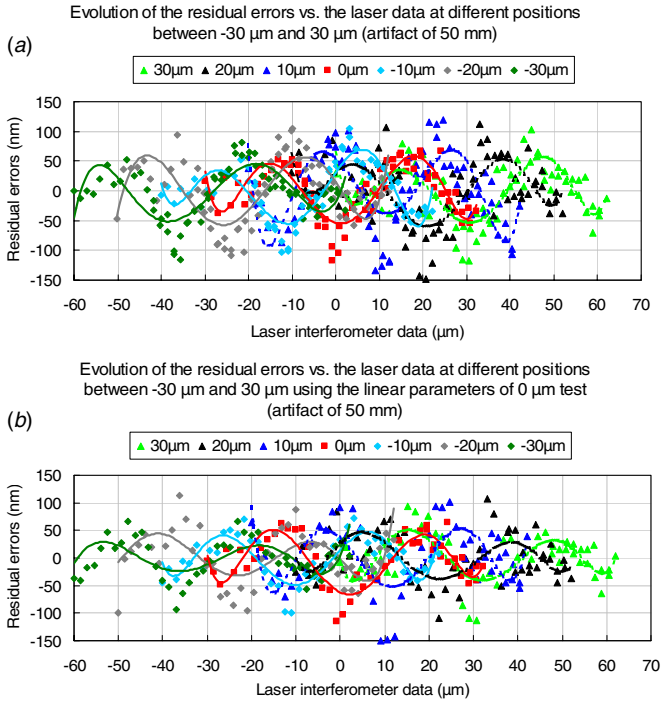

Figure 16. (*a*) Evolution of the residual errors when the 350 μm chromatic confocal probe is focused on the 50 mm cylinder at different transverse positions versus the interferometer data. (*b*) Evolution of the residual errors when using the 0 μm model versus the interferometer data from -30 to 30 μm.

The residual errors are obtained for the entire travel range and present a Gaussian distribution (figure 18). The residual errors

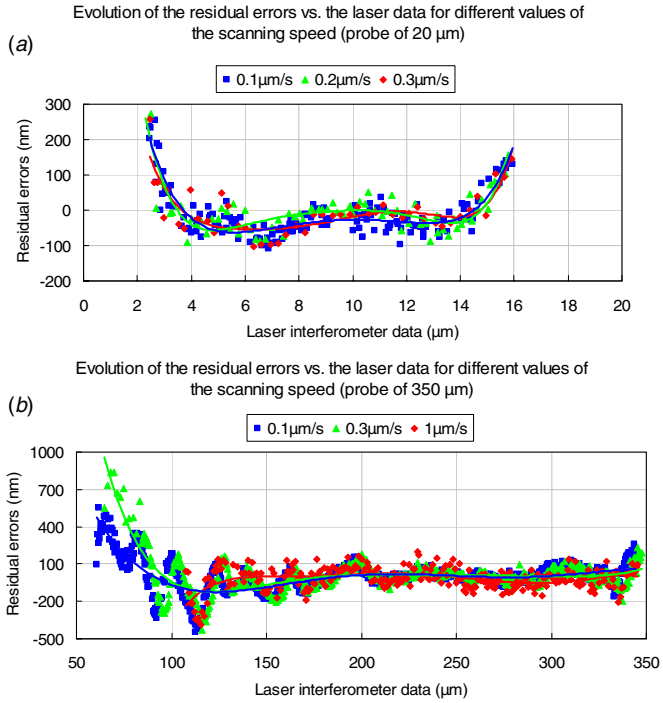

Figure 17. (*a*) Evolution of the residual errors when the 20 μm chromatic confocal probe is used with continuous functioning mode for the speed values of 0.1, 0.2 and 0.3 μm s^{-1}. (*b*) Evolution of the residual errors when the 350 μm chromatic confocal probe is used with continuous functioning mode for the speed values of 0.1, 0.3 and 1 μm s^{-1}.

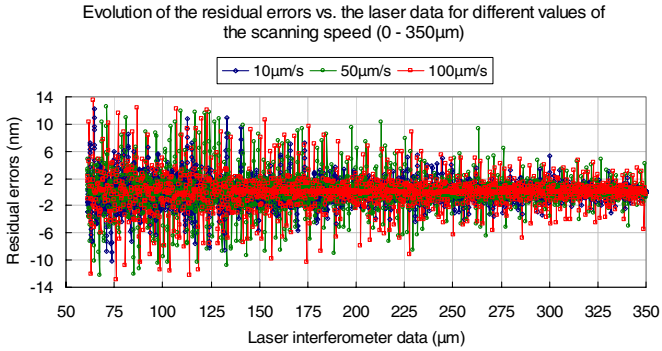

Figure 18. *In situ* calibration of the optical chromatic confocal probe of 350 μm on the ultra-high-precision profilometer. Evolution of the residual errors versus the displacement measured by the z-differential laser interferometer (three values of speed of scanning).

are less than 14 nm at the beginning of the travel range (0 μm) and decrease to 4 nm at the travel range's end (350 μm).

By using this technique, it is possible to considerably reduce the values of the residual errors to a few nanometres, which is very beneficial when performing measurements at the nanometric level of uncertainty. However, this solution neglects some of the error sources and needs to be able to process a large number of linear models in real time.

Increasing the scanning speed from 10 to 100 μm s^{-1} does not influence the evaluation of the residual errors, which provides the possibility of performing quick measurements with a similar level of accuracy. When using the chromatic

confocal probe of 350 μm over a partial travel range of 150 μm, the uncertainty of the high-precision profilometer is evaluated to 80 nm.

8. Conclusion

This paper illustrates an accurate calibration bench to characterize nano-scale optical probes. Based on the literature review and in order to perfectly reach the desired accuracy for the bench, two laser interferometers are used as references. The basic design principles are respected: metrology loop optimization and the Abbe principle, and specific materials were carefully selected. To estimate the uncertainty budget, several sources of error are considered: thermal expansion, uncertainty in the interferometric measurement and uncertainty related to the chromatic confocal probe motion performed by the motor and the piezoelectric actuator.

Different experimental tests are performed when changing: material, surface roughness, colour, inclination angles and sample geometry. The results reveal that the chromatic confocal probe of 20 μm is sensitive to colour. However, the chromatic confocal probe with larger measuring range is less influenced by the material, the colour and the roughness of the sample. The impact of shape of the sample on the behaviour of the two chromatic confocal probes is also investigated by using two cylindrical artefacts of diameters 50 and 75 mm, respectively. When the diameter of the artefact decreases, meaning that the curvature increases more rapidly as the probe scans further from the generatrix, the amplitude of the noise increases, and inversely. The impact of the scanning speed is also studied and influences the residual errors and the working range of the chromatic confocal probes.

Based on the obtained results, chromatic confocal probes can be used to perform measurements with an accuracy of a few hundred nanometres. To minimize the amplitude of the residual errors to less than 15 nm, a partial linearization of the data is done. Then, for the 350 μm working range of the chromatic confocal probe, 2048 partial linear models are calculated to cover the whole travel range. This solution is helpful in reducing the residual errors of the probe without giving any software correction, but then, a large number of linearization parameters have to be processed.

Acknowledgments

The authors sincerely thank the EMRP organization. The EMRP is jointly funded by the EMRP participating countries within EURAMET and the European Union (IND10).

References

[1] Vaissiere D 2003 Métrologie tridimensionnelle des états de surface par microscopie confocale à champ étendu *PhD Thesis* University of Strasbourg
[2] International Organization for Standardization 2010 Geometrical product specification (GPS)—surface texture: areal—part 6. Classification of methods for measuring surface texture ISO 25178-6 2010
[3] Charron J 1999 *Mesure Sans Contact: Etat de l'Art* (Neubiberg: CeTIM)
[4] Leach R 2011 *Optical Measurement of Surface Topography* (Berlin: Springer)
[5] Wilson T 1990 *Confocal Microscopy* (London: Academic)
[6] Schwenke H *et al* 2002 Optical methods for dimensional metrology in production engineering *CIRP Ann.* **51** 685–99
[7] Cacace L A 2009 An optical distance sensor tilt robust differential confocal measurement with mm range and nm uncertainty *PhD Thesis* Eindhoven University of Technology
[8] International Organization for Standardization 2010 Geometrical product specification (GPS)—surface texture: areal—part 602. Nominal characteristics of non-contact (chromatic confocal probe) instruments ISO 25178-602 2010
[9] Boltryk P J, Hill M, McBride J W and Nasce A 2008 A comparison of precision optical displacement sensors for the 3D measurement of complex surface profiles *Sensors Actuators* A **142** 2–11
[10] Boltryk P J, Hill M and McBride J W 2009 Comparing laser and polychromatic confocal optical displacement sensors for the 3D measurement of cylindrical artefacts containing microscopic grooved structures *Wear* **266** 498–501
[11] Nouira H *et al* 2014 Setup of a high-precision profilometer and comparison of tactile and optical measurements of standards *Meas. Sci. Technol.* **25** 044016
[12] Vissiere A *et al* 2012 Concept and architecture of a new apparatus for cylindrical form measurement with a nanometric level of accuracy *Meas. Sci. Technol.* **23** 094014
[13] Vissiere A *et al* 2012 A newly conceived cylinder measuring machine and methods that eliminate the spindle errors *Meas. Sci. Technol.* **23** 094015
[14] Joint Committee for Guides in Metrology 2008 Evaluation of measurement data—guide to the expression of uncertainty in measurement *JCGM 100:2008* (GUM 1995 with Minor Corrections) (Joint Committee for Guides in Metrology)
[15] Stone J, Phillips S and Mandolfo G 1996 Corrections for wavelength variations in precision interferometric displacement measurements *J. Res. Natl Inst. Stand. Technol.* **101** 671–4
[16] Goshtasby A 1988 Image registration by local approximation methods *Image Vis. Comput.* **6** 2552–61
[17] Forsythe G 1957 Generation and use of orthogonal polynomials for data-fitting with a digital computer *J. Soc. Ind. Appl. Math.* **5** 74–88
[18] Nouira H *et al* 2013 Metrological characterization of optical confocal sensors measurements *Met & Props'13: 14th Int. Conf. on Metrology and Properties of Engineering Surfaces (Taipei)*